Agilent | Trusted Answers

Calling all Academia customers! Don't miss this opportunity to buy a new UV-VIS/NIR

Calling all Academia customers!

Now is a great time to invest in UV-Vis/NIR and with the Agilent Cary 5000 you will find the ideal choice for your research.
For a limited time only we are offering you a **great promotion*** on our Cary 5000 and our integrating sphere accessory combined, the perfect package for UV/Vis NIR research.
If your research involves the analysis of **photovoltaic cells**, t**hin films, semiconductor materials and more**, then the Cary 5000 is a great instrument to advance your research

Discover more

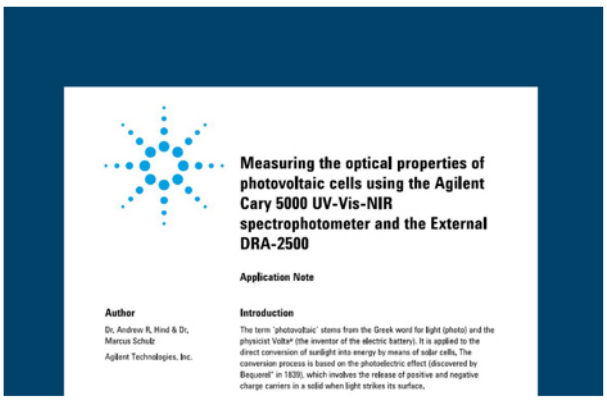

Measuring the optical properties of photovoltaic cells using the Agilent Cary 5000 UV-Vis-NIR spectrophotometer and the External DRA-2500

Application Note

Author

Dr. Andrew R. Hind & Dr. Marcus Schulz

Agilent Technologies, Inc.

Introduction

The term 'photovoltaic' stems from the Greek word for light (photo) and the physicist Volta* (the inventor of the electric battery). It is applied to the direct conversion of sunlight into energy by means of solar cells. The conversion process is based on the photoelectric effect (discovered by Bequerel* in 1839), which involves the release of positive and negative charge carriers in a solid when light strikes its surface.

Learn more with our application note

"Measuring the optical properties of photovoltaic cells using the Agilent Cary 5000 UV-VIS-NIR spectrophotometer and the External DRA-2500"

*Terms and Conditions: Refer to promotion code 1678. Offer valid until the 12th April 2021. Full T&C on can be seen on the website

Agilent | Trusted Answers

Check for updates

Received: 14 November 2019 | Revised: 24 March 2020 | Accepted: 26 March 2020

DOI: 10.1002/rcm.8797

RESEARCH ARTICLE

Rapid Communications in Mass Spectrometry WILEY

Practical considerations for improved reliability and precision during determination of $\delta^{15}N$ values in amino acids using a single combined oxidation–reduction reactor

Philip M. Riekenberg[1] | Marcel van der Meer[1] | Stefan Schouten[1,2]

[1]NIOZ Royal Netherlands Institute for Sea Research, Marine Microbiology and Biogeochemistry Department, Utrecht University, Den Burg, The Netherlands

[2]Faculty of Geosciences, Utrecht University, Utrecht, The Netherlands

Correspondence
P. M. Riekenberg, NIOZ Royal Netherlands Institute for Sea Research, Marine Microbiology and Biogeochemistry Department, Utrecht University, P.O. Box 59, 1790AB Den Burg, The Netherlands.
Email: phrieken@gmail.com

Rationale: There has been increased interest in the measurement of $\delta^{15}N$ values in amino acids (AAs) to gain simultaneous insight into both trophic relationships and the composition of biogeochemical sources used by producers at the base of the food web. A new combustion reactor design in gas chromatography/combustion isotope ratio mass spectrometry (GC/C-irMS) equipment has brought to light variable outcomes in performance, highlighting the need for better information about best practices for new systems.

Methods: Precision for $\delta^{15}N$ values in amino acids using the single combined oxidation–reduction reactor is improved across a sequence of analyses if the reactor is oxidized for a substantial period (2 h) and subsequently maintained throughout the sequence with 12–17 s seed oxidation before each run during GC/C-irMS. A five-point calibration curve using amino acids with a range of $\delta^{15}N$ values from −2.4‰ to +61.5‰ was used in combination with a 13–15 amino acid mixture to consistently normalize measurements to internationally calibrated reference materials.

Results: Combining this oxidation method with normalization techniques using both internal and external standards provided a reliable throughput of ~25 samples per week. It allowed for a reproducible level of precision of <±0.5‰, n = 10 within a derivatized standard mixture across each sequence and an average sample precision of ±0.27‰ n = 3, which is lower than the analytical precision typically associated with $\delta^{15}N$ values for amino acid analysis (<±1‰).

Conclusions: A few practical considerations regarding oxidation and conditioning of the combustion reactor allow for increased sequence capacity with the single combined oxidation–reduction reactor. These considerations combined with normalization techniques result in a higher throughput and reduced analytical error during the measurement of $\delta^{15}N$ values in amino acids.

1 | INTRODUCTION

Ecologists, physiologists, archaeologists, and paleoceanographers are showing increasing interest in the additional information that trophic and source amino acid $\delta^{15}N$ values can provide to further clarify poorly characterized resource contributions that often arise while measuring bulk $\delta^{13}C$ and $\delta^{15}N$ values in ecosystem research.[1–5] Difficulties can arise when variability in the underlying $\delta^{15}N$ values for

 © 2020 John Wiley & Sons, Ltd.

resources supporting primary producers is poorly constrained or not possible to reconstruct (e.g., historical ecology) for an ecosystem. Shifts in underlying basal resource δ^{15}N values make it impossible to disentangle changes in trophic position and source mixing in systems without additional information about primary producers. However, determination of δ^{15}N values from protein-derived amino acids has allowed for the classification of amino acids into source and trophic groups providing additional information about the underlying isotopic composition of the N sources being utilized within the ecosystem as well as refining estimates for trophic position that is not available from traditional bulk measurement of δ^{15}N values.[6]

Source amino acids (AAs) undergo little to no isotopic fractionation during metabolism due to minimal exchange with the metabolic amino acid pool[7] leaving amino acid δ^{15}N values that largely reflect the isotopic composition of the N sources within the environment where the animal resided as the tissue was formed.[8–10] Trophic AAs undergo considerable isotopic fractionation as they are metabolized via transamination[11] resulting in an apparent stepwise increase in δ^{15}N values that corresponds to the trophic level of the animal.[11,12] The difference in δ^{15}N values between source and trophic AAs can thus be used to calculate trophic position (TP), a baseline-normalized estimate of the trophic level of that individual within the local food web. It is common to use either the δ^{15}N values of glutamic acid (Glu) as a trophic amino acid and phenylalanine (Phe) as a source amino acid[1,4,6,9] or a combination of several trophic and source AAs.[11,12] Increasing stepwise differences occur between trophic and source AAs in animals that correspond to TP.[4,6,12,13] These incremental differences between TPs allow for quantification of (a) the trophic discrimination factor (TDF), the per mil differences between TPs within an ecosystem, and (b) β, the per mil difference between the δ^{15}N values of trophic and source AAs in primary producers. Error values associated with TDF (±2.5‰)[13] and β (±0.9‰)[4] are considerably larger than or comparable with the currently accepted measurement error (<±1‰) for δ^{15}NAA analysis.[14]

δ^{15}N values of amino acids are generally measured using gas chromatography/combustion isotope ratio mass spectrometry (GC/C-irMS), which involves three steps to isolate and prepare samples for analysis: (a) release of free and bound AAs from a tissue, (b) isolation of AAs from contaminating matrix materials, and (c) derivatization to facilitate the interaction of AAs with the chromatography column for separation.[1] Acid hydrolysis of proteinaceous tissue generally occurs through heating the sample material in a strong acid to 100°C–150°C for 1.5–10 h, thereby breaking peptide bonds and releasing the individual AAs from the proteins contained in the sample material.[15] Isolation of AAs from interfering sample material is performed if samples contain a complex matrix (e.g., bone, sediment, and carbonates) that can interfere with the analysis and is commonly performed using cation-exchange chromatography.[10,16] The use of a cation-exchange resin generally results in minimal isotopic fractionation of AAs and provides sufficient recovery of sample material to allow analysis.[17] Before analysis, the AAs should be derivatized to reduce polarity and increase volatilization of the compounds. Derivatization allows for increased chromatographic separation, and several derivatization agents can be used to prepare AAs for analysis, for example, trifluoroacetyl-isopropyl ester,[18,19] pentafluoropropyl isopropyl esters,[20] pivaloyl-isopropyl ester,[6] or methoxycarbonyl AA ester.[21] The derivatization agent used depends on the application, and the choice of agent should be explored with consideration toward target AAs, whether δ^{13}C or δ^{15}N values are desired, the relative stability of the derivatized compounds, and whether the introduction of halogenated compounds during GC/C-irMS is necessary.[1,14]

After the isolation and derivatization of AAs, they are analyzed using GC/C-irMS through column separation followed by combustion and then reduction. A traditional GC combustion/reduction interface for irMS uses two reactors: first a Cu/NiO/Pt oxidation reactor heated to 950°C –1000°C that allows for combustion, followed by a Cu reduction reactor heated to 550°C –650°C that primarily reduces NO_x products produced during combustion. Common problems encountered during the determination of δ^{15}N values for AAs via the two separate reactor systems include considerable overloading of AA carbon on the GC column as well as the combustion reactor, incomplete combustion, incomplete reduction, leakage (high background N_2), and issues with standardization to correct for drift (increasing δ^{15}N value) occurring across runs. Overloading of AA carbon during the determination of δ^{15}N values is expected as there is ~18× more carbon produced to obtain N_2 for AA analysis (~9× more C than N in AAs and 2 AAs usually required to produce N_2). Therefore, a considerable mass of AAs must be loaded during GC/C-irMS studies to produce adequate N sample peaks for analysis. Consistent carbon overloading leads to relatively quick degradation of peak shape from the pre-column, quicker degeneration/clogging of the combustion reactor, and the requirement for more frequent oxidation (and ultimately replacement) of the reactor to maintain combustion capacity. Incomplete reduction results in the appearance of considerable mass 30 signal (*m/z* 30, Figure 1A) derived from the formation of NO_x, and regularly occurs after the oxidation periods (<2 min to >60 min) that are required to recover reactor combustion capacity. Leakage within the gas chromatograph is also a routine problem due to development of leaks in connections during repeated heating cycles, and results in regular downtime. Proper standardization across daily sequences is important to correct for drift in δ^{15}N values that can occur as the oxidation state of the combustion reactor changes across the day.

The combined effect of these difficulties results in a low sample throughput, whereas ecological studies examining stable isotopes often involve large sample sizes for many species within food webs (e.g., Christianen et al[22]). A combined oxidation–reduction reactor that contains a nickel oxide tube with CuO/NiO/Pt wires is now routinely used for the analysis.[14,23] Here we discuss the optimization of the combined oxidation–reduction reactor system for the determination of δ^{15}N values of *N*-pivaloyl-amino acid- i-propyl esters through making a few practical changes to the daily sequence of analysis (e.g., length of seed oxidation, daily oxidation period of 2 h, and targeted loading concentrations for both standards and samples). In addition, we optimized the performance of the oxidation–reduction reactor by

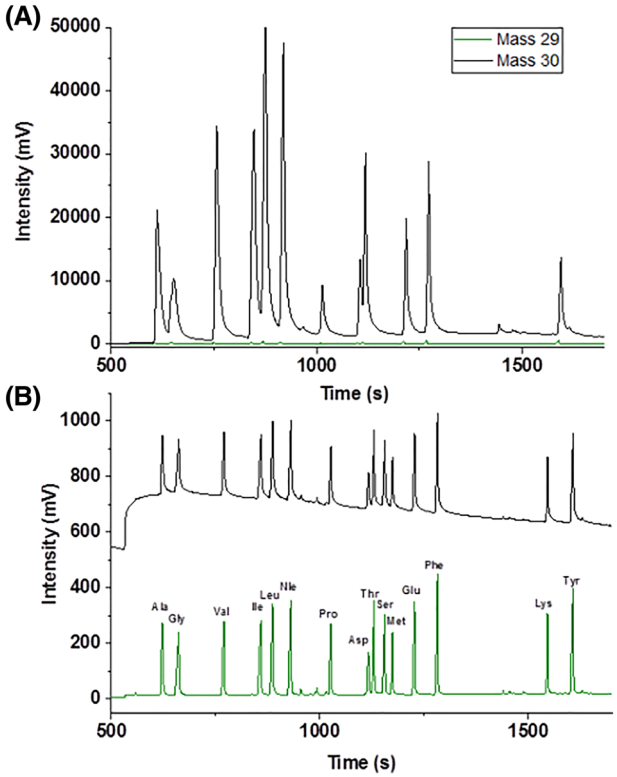

FIGURE 1 Chromatograms for AA standards run immediately after A, oxidation of the combustion reactor on the GC combustion III interface and B, oxidation, backflush, and conditioning for the single combined oxidation–reduction reactor and Isolink II interface. Note the difference in the *y*-axis scale between the two plots. For acronyms of amino acids, see main text [Color figure can be viewed at wileyonlinelibrary.com]

examining the relationship between peak areas and δ^{15}N values while incrementally increasing the seed oxidation length (7 s–22 s). After the optimization of oxidation conditions during analysis, we were able to considerably increase sample throughput while achieving increased precision for the determination of δ^{15}N values of individual AAs.

2 | MATERIALS

2.1 | Reagents and reference materials

Individual amino acids (L- form, >98% purity) were purchased (Sigma Aldrich, Darmstadt, Germany and Arndt Schimmelmann, Indiana University, Bloomington, IN, USA), and reference standard mixtures were created in-house. A mixture of five AAs with a known large range in δ^{15}N values (−2.4‰–61.5‰; Table S1, supporting information) and the internal reference standard L-norleucine (Nle) was used for scale normalization, and will be referred to as the "scaling AA mix". This mixture consisted of approximately equimolar quantities of alanine (Ala), glutamic acid (Glu), glycine (Gly, USGS65; USGS, Reston, VA, USA), phenylalanine (Phe), Nle, and valine (Val, USGS74) prepared in 0.1 M HCl to a concentration of ~44 mM. A second mixture of 14 AAs and the internal reference standard (Nle) was used as a reference standard to calculate offsets occurring during derivatization and combustion during analysis and will be referred to as the "offset AA mix". This standard consisted of approximately equimolar quantities of Ala, aspartic acid (Asp), Glu, Gly, leucine (Leu), lysine (Lys), isoleucine (Ile), methionine (Met), Phe, threonine (Thr), tyrosine (Tyr), serine (Ser), and Val prepared in 0.1 M HCl to a concentration of ~8.8 mM. The δ^{15}N value of each AA used in this mixture was established via direct measurements using elemental analyzer isotope ratio mass spectrometry (EA-irMS) (Table S1, supporting information). An internal reference spike of L-Nle for inclusion into samples after acid hydrolysis was prepared at 44.8 mM in 0.1 M HCl. All three solutions were stored in the dark at −20°C.

The solvents and reagents for acid hydrolysis and derivatization included acetyl chloride (>99%, Fluka, Seelze, Germany), bi-distilled water, hydrochloric acid (VWR International, Boxmeer, The Netherlands), magnesium sulfate (99.5% min, anhydrous; Alfa Aesar, Waltham, MA, USA), trimethylacetyl chloride (>98%; Alfa Aesar), and HPLC-grade dichloromethane (DCM), ethyl acetate, hexane, isopropanol, and methanol (Promochem, Berlin, Germany).

2.2 | Sample materials

Sample materials analyzed included muscle tissue from brown shrimp (*Crangon crangon*), green crab (*Carcinus maenas*), European bass (*Discentrarchus labrax*), blue mussel (*Mytilus edulis*), Pacific oyster (*Crassostrea gigas*), European plaice (*Pleuronectes platessa*), and harbor porpoise (*Phocoena phocoena*) collected from the Wadden Sea. Whole body tissue excluding the gut was used for ragworm (*Hediste diversicolor*), and plankton (<200 μm mesh, filtered seawater) was sampled from the water column of the sublittoral zone at the Marsdiep, The Netherlands (N 53° 0′ 13″, E 4° 46′ 26″). The plankton sample was a mixture of detritus, zooplankton, and phytoplankton, but was dominated by large microalgae confirmed by light microscopy and a bulk δ^{13}C value of −21.2‰. All samples excluding harbor porpoise and plankton were collected as part of the synoptic intertidal benthic surveys (SIBES) from 2011 to 2013 using the same methods as presented in Christianen et al.[22] Materials were freeze-dried for 48 h and homogenized before analysis. The samples reflect a cross section of the Wadden Sea food web with representatives from several TPs, including primary producer, primary consumer, omnivore, and apex predator.[22]

3 | PROCEDURE

3.1 | Amino acid isolation and preparation

An amount of 3–5 mg of freeze-dried, ground, and homogenized tissue was acid hydrolyzed (100°C) for 10–12 h and subsequently filtered (0.45 μm), lipid extracted, and spiked with the internal reference standard Nle following the sample protocol presented in

Svensson et al[24] and Chikaraishi et al.[4] The hydrolysates were subsequently evaporated under N_2 gas to dryness and then isopropylated with a mixture of isopropanol and acetyl chloride (3/2, v/v) heated to 100°C for 2 h (heating block set at 124°C with an independent thermometer set into a reaction vial to confirm the internal reaction temperature). The hydrolysate was then evaporated to dryness (40°C, using N_2); to this dried hydrolysate a mixture of hexane and DCM (3/2, v/v) was added and the resulting mixture was evaporated to dryness (40°C, using N_2) twice to remove any remaining reagent. The AA *i*-propyl esters were then acylated using a mixture of trimethylacetyl chloride and DCM (1/4, v/v) by heating to 100°C for 2 h to obtain *N*-pivaloyl-amino acid-i-propyl esters. The prepared esters were volatile at this point and were allowed to evaporate to dryness at 40°C under a gentle stream of N_2; to this dried product, a mixture of hexane and DCM (3/2, v/v) was added and the resulting mixture was then evaporated to dryness (40°C, using N_2) twice to remove any remaining reagent. The dried material was then solvent extracted using bi-distilled water and a hexane/DCM mixture (3/2, v/v), with the solvent gently evaporated to dryness (40°C, using N_2). The *N*-pivaloyl-amino acid-i-propyl esters were stored frozen (−20°C) and resuspended in ethyl acetate before analysis. Prepared *N*-pivaloyl-amino acid-i-propyl esters extracts have an expected storage capacity of <12 weeks,[25] and all samples in this study were analyzed within 1 month of being derivatized. Additional details are provided in Supplementary Material 1 (supporting information).

3.2 | Analysis via GC/C-irMS

Analyses were performed using a Thermo Trace 1310 gas chromatograph connected to a Delta V Advantage irMS instrument via a GC IsoLink II combustion interface (all supplied by Thermo Fisher Scientific, Bremen, Germany) using the ramp schedule and materials detailed in Supplementary Material 1 (supporting information). This analysis uses an oxidation–reduction reactor consisting of a NiO tube containing CuO/NiO/Pt wires within an aluminum oxide tube continuously heated to 1000°C during operation. The oxidation capacity of the reactor was ensured before each sequence by oxidation for 2 h, followed by a backflush period (30 min) to remove any unwanted oxidation products (NO_x monitored at *m/z* 30). During the day-to-day analysis a sequence of 25 runs was used consisting of 5 samples run in duplicate, 2 "scaling mix" standards, 10 "offset AA mix" standards, and an alkane mix run immediately after the long daily oxidation. During the oxidation optimization, a sequence of 16 runs was used consisting of 2 samples run in triplicate with 2 "scaling AA mix" standards, 7 "offset AA mix" standards, and an alkane mix run immediately after the long daily oxidation. Throughout both sequences, the "offset AA mix" bookended sample duplicates or triplicates. The combustion reactor was conditioned after oxidation by a single injection of alkanes suspended in ethyl acetate (~equimolar quantities of C_{17}, pristane, C_{18}, C_{20}, C_{28}, C_{30}, and C_{32}; ~25 ng uL^{-1}), and the oxidation capacity was maintained throughout the sequence by a seed oxidation (12–17 s) before each run during the sequence. Flow rates (GC column + backflush flows, GC column flow, and GC column + backflush + oxygen flows) measured via an internal flow meter and free O_2 (monitored at *m/z* 32) were closely monitored between sequences as indicators of declining reactor oxidation capacity or potential blockage across the lifetime of the reactor. Using this oxidation program, *m/z* 30 was held to acceptable levels that did not interfere significantly with $\delta^{15}N$ values across the run (standard deviation <±0.5‰ for 13 AAs across 10 runs of the internal AA standard mix in each sequence) and remained relatively low across sequences (*m/z* 30 < 700 mV, ratio of *m/z* 30/*m/z* 28 ~ 5%).

To prevent interference with the measurement of N_2 in the source, CO_2 was removed post combustion by a liquid N_2 trap. CO_2 was emptied from the trap before the 2 h oxidation and the capillary remained outside the trap until after conditioning with *n*-alkanes was finished. As long as overloading of sample concentration did not occur, there was sufficient capacity within the CO_2 trap to hold CO_2 across the entire sequence of 25 runs without emptying. To avoid overloading of the column and CO_2 trap, all samples were first run on a GC-flame ionization detector to identify the relative amount of C contained in the samples, to target sample dilutions before analysis using GC/C-irMS.

3.3 | Data analysis and normalization

The $\delta^{15}N$ values of underivatized AAs included in standard mixes for normalization of GC/C-irMS data were determined using EA-irMS (EA-δ^{15}NAA; Table S1, supporting information). Multiple analyses of each AA were performed on a Flash 2000 elemental analyzer connected to a Delta V Advantage irMS instrument via a Conflo IV interface (all from Thermo Fisher Scientific) and were calibrated on IAEA-N-1 and IAEA-N-2 using the secondary reference materials acetanilide #1 and urea #2 ($\delta^{15}N$ values of 1.18 ± 0.02‰ and 20.17 ± 0.06‰, respectively).[26] The precision for this analysis is ±0.1‰.

Derivatized samples are routinely analyzed in duplicate during GC/C-irMS, but during the oxidation optimization process in October 2019, the samples were analyzed in triplicate. Normalization and scaling for samples and standards followed the calculations presented in Yarnes and Herszage[14] and were applied to each sequence. This method uses a set of three corrections to normalize the data produced through the use of (a) an internal reference spike (Nle) included in all samples and standard mixtures and that undergoes the same derivatization, combustion, and reduction process; (b) an AA mixture used to calculate an offset for each individual AA resulting from derivatization; and (c) a scaling standard mixture using AAs with a large range of $\delta^{15}N$ values calibrated against international standards. First, all samples and standard mixtures were evaluated against the internal reference spike instead of the laboratory reference monitoring gas due to the principle of identical treatment. Subsequently, a corrected value ($\delta^{15}NAA_{Off}$) that accounted for

derivatization was calculated for all 13-14 AAs in the reference mixtures using the equation:

$$\delta^{15}NAA_{Off} = \text{measured}\,\delta^{15}NAA - \delta^{15}NAA_i \quad (1)$$

where $\delta^{15}NAA_i$ = measured $\delta^{15}NAA$ – known $\delta^{15}NAA$ for each amino acid in the 13 AA mixture. The $\delta^{15}NAA_{Off}$ values were then normalized to international reference standards by performing a linear regression of the measured $\delta^{15}NAA_{Off}$ values and the known values of the "scaling AA mix" and using the resulting equation to correct the offset-adjusted sample values to an internationally calibrated scale across all five AAs included in the "scaling AA mix" as:

$$\delta^{15}NAA_{scaling} = m*\delta^{15}NAA_{Off} + b \quad (2)$$

where m is the slope and b is the intercept of the regression across all five AAs. The materials used for each correction are (a) Nle, (b) "offset AA mix", and (c) "scaling AA mix" ($\delta^{15}N$ values ranging from −2.4‰ to +61.5‰; Ala, Glu, Gly, Phe, and Val; Arndt Schimmelmann). The $\delta^{15}N$ values are all presented as "per mil" (‰) relative to atmospheric nitrogen as determined by the International Atomic Energy Agency (IAEA, Vienna, Austria).

3.4 | Statistics

In each sequence, samples and "scaling AA mix" were run in duplicate. "Offset AA mix" values are reported as mean ± standard deviation across each sequence (n = 10). Linear regressions were used to calculate the scaling corrections to internationally calibrated standards (see above). The separation index was calculated as:

$$Rt_2 - Rt_1/0.5 \times (W_1 + W_2) \quad (3)$$

where Rt is the retention time and W is the width for each of the peaks being compared. TP estimates were made using normalized measurements for Glu and Phe within individual samples and calculated as:

$$TP = 1 + \left(\delta^{15}N_{Glu} - \delta^{15}N_{Phe} - \beta\right)/TDF_{Glu-Phe} \quad (4)$$

where $\delta^{15}N_{Glu}$ and $\delta^{15}N_{Phe}$ are the $\delta^{15}N$ values for Glu and Phe in the sample, and TDF and β are set at 7.6 ± 2.5‰ and 3.4 ± 0.9‰, respectively.[4,13]

4 | ASSESSMENT

4.1 | Conditioning and monitoring of reactor performance

Our previous method for measuring the $\delta^{15}N$ values of amino acids used separate oxidation and reduction reactors in a GC combustion III system (Thermo Fisher Scientific). In this current method, oxidation by flushing O_2 was used to improve and maintain combustion capacity only sparingly when the peak shape deteriorated (e.g., tailing, reduced peak height). This was due to the considerable increase in m/z 30 intensity (from NO_x) that interfered with measurement of $\delta^{15}N$ values and loss of intensity of m/z 28 and 29 (from N_2) that occurred after this oxidation (Figure 1A, m/z 30, 10–50 V). After oxidation, recovery of m/z 29/28 required multiple injections of N-containing compounds (e.g., tributylamine, AA standard mix, n = 5–20) to condition both reactors and resulted in a considerable loss of analysis time to recover the measurement baseline for m/z 30 (0.5–2 days). Here, using the combined oxidation and reduction reactor in the Thermo Fisher Scientific IsoLink II system, it was necessary to include an extended oxidation period at the beginning of the daily sequence before standard and sample analysis. Daily extended oxidation resulted in predictable oxidation capacity from the reactor and m/z 29/28 across sequences for the 2-month analytical period presented here (80 samples in duplicate; 160 standards; 16 sequences). In addition, we present a quantitative optimization of oxidation performance performed directly after the installation of a new reactor for routine analysis to demonstrate a procedure for establishing optimal oxidation conditions for other laboratories. These findings represent a significant improvement in precision, reliability, and laboratory throughput of $\delta^{15}NAA$ samples solely due to practical considerations built into routine analysis procedures. Subsequently, we have observed the maintenance of precision and reliability for this method across >1400 standards and 600 samples using three reactors with an average lifetime of ~60 sequences each.

To obtain a predictable oxidation capacity from the combined oxidation–reduction reactor, we used a combination of an extended initial oxidation, followed by conditioning via a mixture of alkanes in ethyl acetate, and subsequently maintained oxidation through a seed oxidation (7, 12, 17, and 22 s) after each run. This strategy resulted in a m/z 30 baseline ranging from <614 ± 63 mV during the analysis of the initial offset standard to >367 ± 25 mV during the analysis for the last "offset AA mix" (the 25th sample in each sequence). The m30 baseline was elevated in a consistent manner across the sequence as evidenced by consistent m/z 29/28 and a precision <0.5‰ between the 7 and 10 "offset AA mix" standards run across each sequence. Consistent reproducibility in the m/z 29/28 across sequences led to a predictable interference (Figure 1B) between sequences across the lifetimes of the three oxidation–reduction reactors that we have used. In contrast, decreased combustion capacity (caused by shorter seed oxidation times) led to an incomplete conversion of the analyte and resulted in a variable increase in $\delta^{15}N$ values and loss of peak areas across sequences (~2‰ 7 and 12 s seed oxidations, peak area ratios <1; Figure 3). Longer seed oxidation times resulted in a progressive decrease in $\delta^{15}N$ values in the standards as sequences progressed (0.7‰–1‰ for 22 s seed oxidation; Figure 3) and caused decreased precision. Optimized performance of the combined oxidation–reduction reactor depends on an oxidation maintenance period that supports complete conversion of the analyte with a minimal decrease in $\delta^{15}N$ values resulting from over-oxidation across the sequence

(Figure 3). Once a balance between these two effects is achieved, the offset across each run in the *m/z* 29/28 ratio becomes relatively consistent across the sequence and allows for a stable correction for this effect through the use of the "offset AA mix" to adjust standard values within each sequence (Figure 2A). Using this optimization for each reactor, we have successfully maintained a precision of <0.5‰ across ~140 sequences (700 samples, n = 2), using the structure of standards (n = 10, 1400 injections; Figure 2) and samples (Table 2), but we present the results for both the standards (n = 7) and the samples (n = 3) used during the optimization procedure for a newly installed reactor (Figure 3; Tables S2 and S3, supporting information). We recognize that reactors behave differently and will potentially need to undergo optimization depending on the variance in the combustion capacity, but we have found that decreasing standard precision (>0.5‰) and peak areas across sequences are the key symptoms that indicate deteriorating reactor conditions.

This performance appears to change little during short-term analysis with shortening of the 2 h daily oxidations. The 30 min backflush after this oxidation appears to be sufficient to return the *m/z* 28/29 to baseline before the analysis of standards regardless of whether a 30 min or 2 h oxidation was used. When using the shorter oxidation period, we did observe small peaks <200 mV occurring during the analysis of the alkane mixture probably from incompletely combusted analyte remaining in the reactor, but the precision for the subsequent "offset AA mix" standards remained unaffected. We have observed similar peaks occasionally after sequences with elevated loading rates of analyte when using the 2 h oxidation, but have not observed any decrease in precision within the sequences that have followed. We have chosen to continue with the daily 2 h oxidation as it has not appeared to adversely affect the reactor lifetimes and ensures that any recalcitrant material remaining in the reactor is sufficiently oxidized regularly to prevent buildup that can lead to premature failure due to clogging. We cannot speak to the reliability of longer-term use of shorter oxidation periods.

In addition, we incorporated into the sequence an ISODAT (Thermo Fisher Scientific) method monitoring *m/z* 32 (O_2) with the backflush turned off between samples and standards. When the oxidation capacity of the reactor was sufficient, *m/z* 32 quickly approached 50 V, but when the oxidation capacity of the reactor was exceeded, *m/z* 32 would only register 10–30 V and the peak retention times retarded with subsequent runs (~5 s). Monitoring *m/z* 32 throughout the sequence allowed for within-sequence monitoring of the reactor oxidation capacity and helped to identify when overloading began to occur.

Furthermore, monitoring carrier gas flow rates before each sequence provided additional information about the long-term state

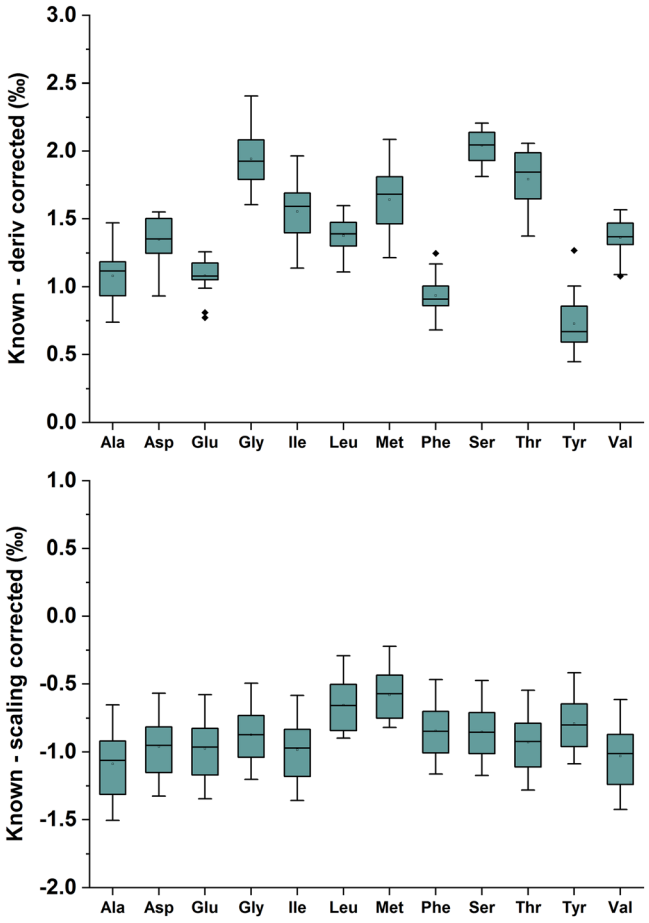

FIGURE 2 Box plots of measured isotopic offsets for a 12 AA standard mixture across 16 daily runs between A, δ^{15}N values measured by EA-irMS for free AAs and by GC/C-irMS corrected for derivatization, and B, δ^{15}NAAi offsets between known δ^{15}NAA values from EA-irMS analysis and δ^{15}NAA values measured using GC/C-irMS corrected for derivatization and scaled to internationally calibrated compound specific standards. Within the boxplots, black dots are the mean, lines represent the median, boxes represent the upper and lower quartiles, and whiskers represent the 1.5 quartile ranges. Any black diamond outside the whiskers is an outlier [Color figure can be viewed at wileyonlinelibrary.com]

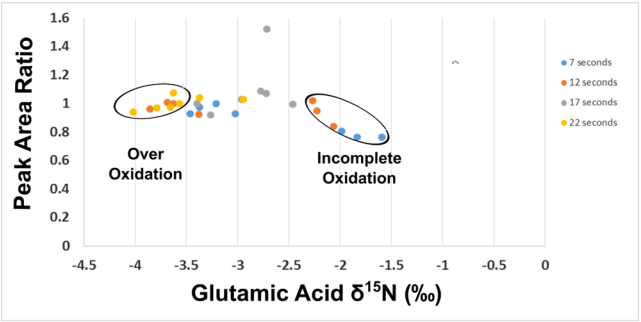

FIGURE 3 δ^{15}N values of glutamic acid vs. peak area ratio for offset standard mix replicates (n = 7) with different lengths of seed oxidation. Peak area ratios below 1 indicate incomplete oxidation and coincide with increase in δ^{15}N values (~2‰, 7 and 12 s seed oxidations) which worsened through the sequences (marked incomplete oxidation, last three replicates of both 7 and 12 s trials, 5 through 7). Additional oxidation resulted in complete combustion as evidenced by the peak areas, but also resulted in decreasing δ^{15}N values with relatively small increases in oxidation times (0.75‰–1‰, 22 second trial) which decreased precision across the sequence [Color figure can be viewed at wileyonlinelibrary.com]

TABLE 1 Retention times and separation indices for analyzed amino acids for both individual methods and a comparison between the two methods

	Svensson et al[24]				This study				Comparison
	Retention time (min)	Width (s)	Amplitude *m/z* 28 (mV)	Separation index	Retention time (min)	Width (s)	Amplitude *m/z* 28 (mV)	Separation index	Separation index
Ala					10.4	12.3	655	2.7	
Gly	17.8	25.5	142	24.0	11.0	11.9	293	7.1	16.9
Val					12.9	14.4	589	5.8	
Leu					14.3	13.8	665	1.9	
Ile					14.8	16.3	513	3.0	
Nle	28.8	29.3	131	50.3	15.5	13.4	749	7.0	20.2
Pro					17.1	16.1	550	7.7	
Asp					18.6	10.9	488	1.1	
Thr					18.8	11.3	427	2.0	
Ser					19.2	15.5	676	1.5	
Met					19.6	14.4	864	4.3	
Glu	49.5	20.1	96	5.6	20.5	11.7	422	3.9	3.9
Phe	51.4	21.5	249	26.0	21.4	13.4	536	20.8	21.2
Lys					25.8	12.5	614	4.5	
Tyr	59.6	16.3	322		26.8	16.1	755		

Note: The separation index is calculated both for the AAs present in each run and for the comparable AAs resulting from each method. Separation index values greater than 1 indicate a difference in peak retention times that is larger than the average width of both peaks. Asp and Thr (1.1) co-eluted at higher standard concentrations, but co-elution was not often observed for peaks with separation index values greater than 1.5.

of the combustion reactor. Declining carrier gas flow rates when the backflush was turned off indicated that clogging of the reactor was beginning to occur, although there was some day-to-day variability in these flow rates (1.56 ± 0.18 mL min^{-1} across the lifetime of the reactor). Directly after analysis, the GC column flow was >1.4 mL min^{-1} (set at 1.6 mL min^{-1}), and the *m/z* 32 peak was >50 V with the backflush turned off. These measurements will vary between systems, but have been included here as an example of the variation in these observations across the lifetime of reactors. We observed that failure of the reactor was characterized by a gradually decreased precision (>0.5‰) for $\delta^{15}N$ values in the "offset AA mix" caused by the increase in standard $\delta^{15}N$ values and lower peak area ratios (Figure 3) toward the end of sequences. This gradual degradation requires standards to be run throughout the sequence to characterize how the oxidation capacity is maintained toward the end of sequence. Our experience is currently limited to the gradual failure of two reactors and does not represent all possible outcomes for reactor failure (e.g., blockage and leakage).

Another consideration for increased reliability across a daily sequence was, before analysis via GC/C-irMS, to analyze samples using GC-flame ionization detector (DB-5MS, Agilent Technologies, Santa Clara, CA, USA; 60 m × 0.32 mm o.d. × 0.5 μm film thickness) to ensure that comparable amounts of sample are injected on column for all samples (Leu > 0.3 μg) based on the relative peak areas for sample vs the internal standard spike (Nle, ~0.3 μg, Table 1). This allowed for targeted dilution for both samples and standards before on-column injection during GC/C-irMS analysis that resulted in *m/z* 29 peak heights of ~300 mV (*m/z* 29 background of 15 mV) for both standards and samples (for Leu, with variations in peaks heights for other AAs depending on tissue type). Maintenance of comparable analyte loading rates allowed the CO_2 trap to remain submerged throughout a sequence (10 "offset AA mix," 2 "scaling AA mix," and 5 samples in duplicate), eliminating any baseline disturbances resulting from the remnants from emptying the trap between runs. When high amounts of analyte are loaded on a column (e.g., accidental evaporation of solvent in a sample vial), the CO_2 trap can become overloaded toward the end of the sequence. Overloading of CO_2 causes increased peak retention times, considerable drift of standard $\delta^{15}N$ values, and decreased precision between standard and sample replicates. Overloading also causes increased co-elution for Asp and Thr and for Ser and Met as the previous peaks increasingly do not come down to baseline. Baseline interferences can be further minimized through targeted loading rates if users are focused on improved accuracy for these amino acids. This method represents a generalized separation with better precision between measurements for a suite of amino acids with acknowledged co-elution potential for a subset of amino acids. Further optimization of ramp temperature, flow rate, and loading should be performed to allow for further separation with a 60 m DB-5 column if users are pursuing particular accuracy for specific problematic AAs. Alternatively, purification of individual AAs using HPLC with subsequent analysis via irMS is a viable option with improved precision for these applications[27] and a direct comparison between this method and the method presented in this study would be useful to the wider community.

4.2 | Normalization

Rather than using solely a single AA mixture to account for both changes in $\delta^{15}N$ values due to derivatization of AAs and long-term stability,[24] we followed the approach of Yarnes and Herszage,[14] which uses three standards to normalize AAs: (a) a spiked AA reference standard (Nle) included in every standard and sample, (b) an AA mixture to account for changes in $\delta^{15}N$ values during derivatization "offset AA mix" (Figure 1B), and (c) an AA mixture to scale to calibrated international standards "scaling AA mix" (Table 1). The precision was within ±0.5‰ for both standard mixes run during the analysis period (5 weeks; 16 sequences; "offset AA mix": 160 injections, average σ ± 0.22‰, range ± 0.18–0.25, min-max: Met-Ala; "scaling AA mix": 32 injections, σ ±0.19, range ± 0.1–0.33, min-max: Val-Gly; Figure 1B and Table 1) as well as the optimization period in October 2019 (Figure 4; and Tables S2 and S3, supporting information). This represents an improvement over the precision of our previously used standard mix (0.7–1.2‰)[24] and the commonly reported precision of ±1‰ for measurement of $\delta^{15}N$ values in AAs.[14,21] Investigating the effects of each correction individually found that the difference between AAs measured using EA-irMS and their derivatives prepared using the NPiP pathway ($\delta^{15}NAA_i$ values) was larger when only corrected to the spiked internal reference standard than for standards that were corrected to the internal reference standard and scale-normalized (1.41 ± 0.18‰ vs −0.88 ± 0.22‰, respectively; Figure 2). Measured differences between AAs measured using EA and their derivatives measured using GC/C-irMS were larger for some amino acids (derivatization offset AA mix: Gly, Thr, and Ser ~2‰, Figure 2; Scaling AA mix: Ala ~2.3‰, Figure 2). Samples that were corrected using this method for normalization had an average precision of (a) 0.18‰ for duplicate measurements during the initial sampling period (0.01–0.49‰ min-max, 12AAs, 7 samples; Table 2) and (b) 0.27‰ for triplicate measurements run during the oxidation optimization (0.04–0.4 8‰, 15 AAs; 2 samples; Table S3, supporting information). All sample measurements have been normalized to internationally calibrated reference materials to ensure comparability with measurements in similarly calibrated analyses.

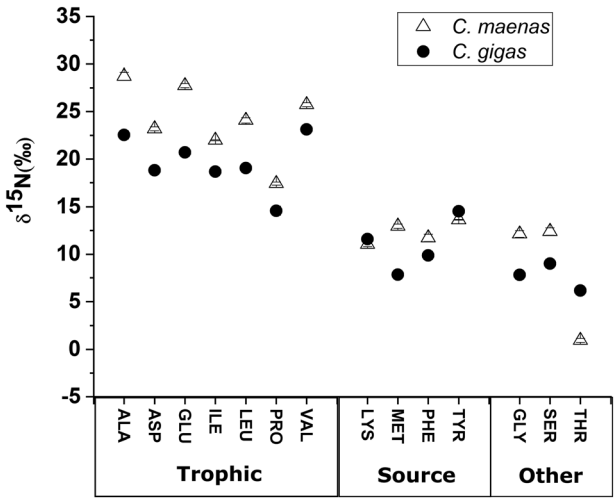

FIGURE 4 $\delta^{15}N$ values for 14 AAs for European green crab (*Carcinus maenas*) and Pacific oyster (*Crassostrea gigas*) assigned to "trophic," "source," and "other" groups based on how they are metabolized. These samples were run in triplicate with a 17 s oxidation using the standards presented in Figure 3. Mean ± SD for triplicate replicates, SD all <0.5 ‰; Table S3 (supporting information); some error bars are too small to be seen

5 | TROPHIC POSITION

In addition to the canonical source and trophic AAs (Phe, Glu), the improved method has allowed $\delta^{15}N$ measurements for other source (Lys, Met, Ser, Tyr), trophic (Ala, Asp, Ile, Leu, Val), and other (Gly, Met, and Thr) AAs with improved precision (±0.5‰, 1σ; Figure 1B, Tables 1 and 2). Improved precision for non-canonical AAs will allow for further reduction of the variability associated with TDF for both consumers and β, as multiple AAs are increasingly used to better constrain variability among AA types,[11,28] or alternative trophic AAs (e.g., Pro) are used for TP measurements.[29,30] The TPs calculated here using Glu and Phe (Equation 4) ranged from 1.3 ± 0.2 for a plankton sample dominated by microalgae to 3.2 ± 0.85 for *D. labrax*, which correlate well with values expected for primary producers and secondary consumers, respectively (Table 2). The error associated with the calculation of TP is primarily a result of the considerable error associated with TDF and β due to physiological variance within the metabolism of individuals and is not considerably reduced with decreased analytical error (±0.21 vs ±0.24 TP using precision ±0.5‰ and ± 1‰, respectively, for phytoplankton using the error propagation formula presented in Okhouchi[1]). Examination of TDF and β within consumer-resource groups with better normalization and decreased analytical error should improve estimates below the current threshold of ±2.5‰ and ±0.9‰ as these variables better reflect physiological and taxonomic variability in biological fractionation.[4,14,31] A reduction of 1‰ in the error estimate for TDF (from 2.5‰ to 1.5‰) halves the propagated error for the TP of secondary consumers (European bass, ±1.1 vs ±0.4, respectively).[1] In addition, improved instrument reliability and reduced downtime allow for increased replication within studies and better efficiency during method development for difficult materials (e.g., microphytobenthos, detrital and sediment trap organic matter).

To demonstrate typical results for the improved method, we analyzed AAs for six species relevant to our current work in the Wadden Sea: *C. crangon*, brown shrimp; *D. labrax*, European bass; *H. diversicolor*, ragworm; *M. edulis*, blue mussel; *P. phocoena*, harbor porpoise; and *P. platessa*, European plaice plus phytoplankton sampled from the Wadden Sea (Table 2, Figure 5). These samples represent an expected range of animals from the Wadden Sea food web that spans from primary producer to apex predator (*P. phocena*). Both the highest and lowest TPs in this study (*D. labrax* and phytoplankton, respectively) demonstrated elevated $\delta^{15}N$ values for the trophic AAs in the secondary consumer compared with the primary producer. The

TABLE 2 δ^{15}N values for NPiP derivatives from acid hydrolysis of tissue of different species from the Wadden Sea after normalization using both internal and scaling AA mix.

	Brown shrimp (*Crangon crangon*)	European bass (*Dicentrarchus labrax*)	Mussel (*Mytilus edulis*)	European plaice (*Pleuronectes platessa*)	Ragworm (*Hediste diversicolor*)	Harbour porpoise (*Phocoena phocoena*)	Plankton
Ala	27.31(0.28)	30.24(0.23)	19.94(0.04)	24.62(0.28)	16.40(0.26)	22.83(0.24)	12.98(0.02)
Asp	22.7(0.20)	26.65(0.26)	16.19(0.05)	23.00(0.16)	15.58(0.01)	23.36(0.15)	14.12(0.41)
Glu	27.65(0.33)	30.16(0.03)	18.26(0.20)	25.52(0.23)	18.56(0.10)	26.00(0.13)	15.79(0.29)
Gly	10.25(0.30)	9.23(0.39)	8.19(0.11)	9.85(0.29)	8.95(0.10)	20.46(0.03)	10.98(0.19)
Ile	18.8(0.30)	26.59(0.11)	18.00(0.29)	22.56(0.10)	15.52(0.08)	20.85(0.29)	10.42(0.06)
Leu	21.29(0.13)	29.89(0.25)	16.73(0.13)	24.37(0.07)	15.64(0.13)	24.96(0.22)	11.54(0.33)
Met	12.47(0.09)	14.12(0.23)	7.60(0.43)	12.48(0.11)	8.40(0.07)	N.D.	N.D.
Phe	10.35(0.01)	10.06(0.36)	7.75(0.09)	10.27(0.35)	6.80(0.21)	12.85(0.22)	10.31(0.02)
Ser	9.87(0.15)	12.49(0.28)	7.34(0.09)	10.80(0.06)	7.23(0.08)	20.06(0.49)	5.73(0.06)
Thr	5.96(0.10)	(−1.4)(0.42)	4.00(0.10)	8.15(0.33)	(−1.96)(0.07)	(−16.79)(0.03)	6.97(0.15)
Tyr	12.76(0.27)	14.52(0.02)	9.14(0.07)	12.27(0.23)	8.46(0.046)	N.D.	8.87(0.11)
Val	22.89(0.27)	29.71(0.32)	18.94(0.07	24.74(0.20)	17.05(0.13)	26.45(0.42)	15.18(0.19)
Glu-Phe	17.29(0.34)	20.10(0.33)	10.52(0.29)	15.25(0.12)	11.76(0.10)	13.15(0.35)	5.48(0.28)
TP	2.8(0.85)	3.2(1.08)	1.9(0.41)	2.6(0.70)	2.1(0.48)	2.3(0.56)	1.3(0.20)

Note: Plankton was material from a bulk water sample retained using a 200 μm mesh size and predominantly consisted of large microalgae. N.D. indicates not determined as the peak heights were below 100 mV and therefore were not suitable for integration.

δ^{15}N values for the source AAs were generally lower, reflecting the smaller fractionation associated with their processing during trophic transfer, with the notable exception of Thr, which was considerably ^{15}N-depleted for the European bass (−1.4‰; Table 2). This negative correlation with elevated TP has been previously observed[11,31,32] and may indicate a strong reverse fractionation associated with trophic transfer of N or be an effect of diet quality or metabolic rate.[2,13] The

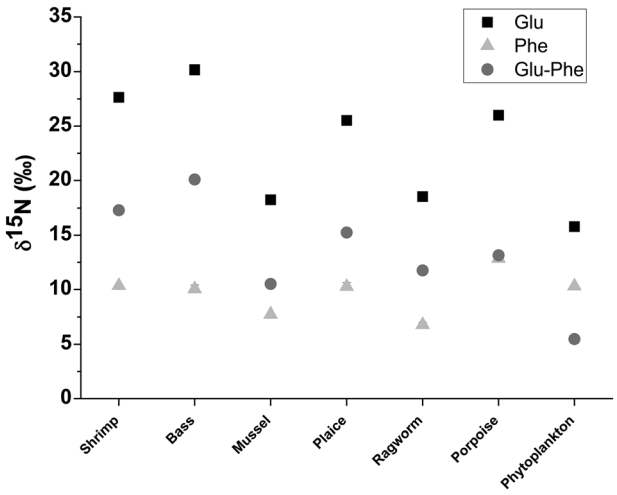

FIGURE 5 δ^{15}N values of glutamic acid and phenylalanine for seven samples as well as the difference that is commonly used in the calculation of trophic position (mean ± SD of analytical duplicates, error bars are too small to be seen)

δ^{15}N value for Gly is relatively close to that of Phe (9.2‰ and 10.1‰, respectively) and may reflect a minimal contribution of microbially degraded material to the diet of European bass[33] or may reflect routing and utilization of Gly as a source AA if Gly is sufficient in the diet.[34] This analytical method reliably produces δ^{15}N values for non-canonical AAs that should allow for further insight into the metabolic processes occurring during trophic transfer of AAs between species.

Comparison between three species, *Cerastoderma edule*, *Arenicola marina*, and *Macoma balthica*, using both the method presented here and the previous method (Svensson et al[24]; Figure 6) showed improved precision for Glu and TP (3.5‰ vs 2.3‰ for Glu and 0.36 vs 0.21 for TP; old vs new, respectively) but decreased precision for Phe (1.7‰ vs 1.9‰; Table S4, supporting information). Increased variability for Phe was driven by the increased variability within *M. balthica* examined using the new method (±1.7‰, n = 8) and probably reflects regional variability in the underlying primary producers supporting this population. Samples were taken from the same sampling sites in the Wadden Sea as part of the SIBES 2011 and 2013 sampling campaigns, but do not include the same individuals for each analysis. Decreased variability was observed primarily due to more consistent standardization techniques that better account for the drift in AA δ^{15}N values that occurred across the daily sequences largely due to interference from *m/z* 29/28. Increased analytical throughput with the new method has allowed for a more routine inclusion of standards throughout the sequence for normalization than was possible or practical with the previous method. In addition, the δ^{15}N values of each individual AA have been standardized to

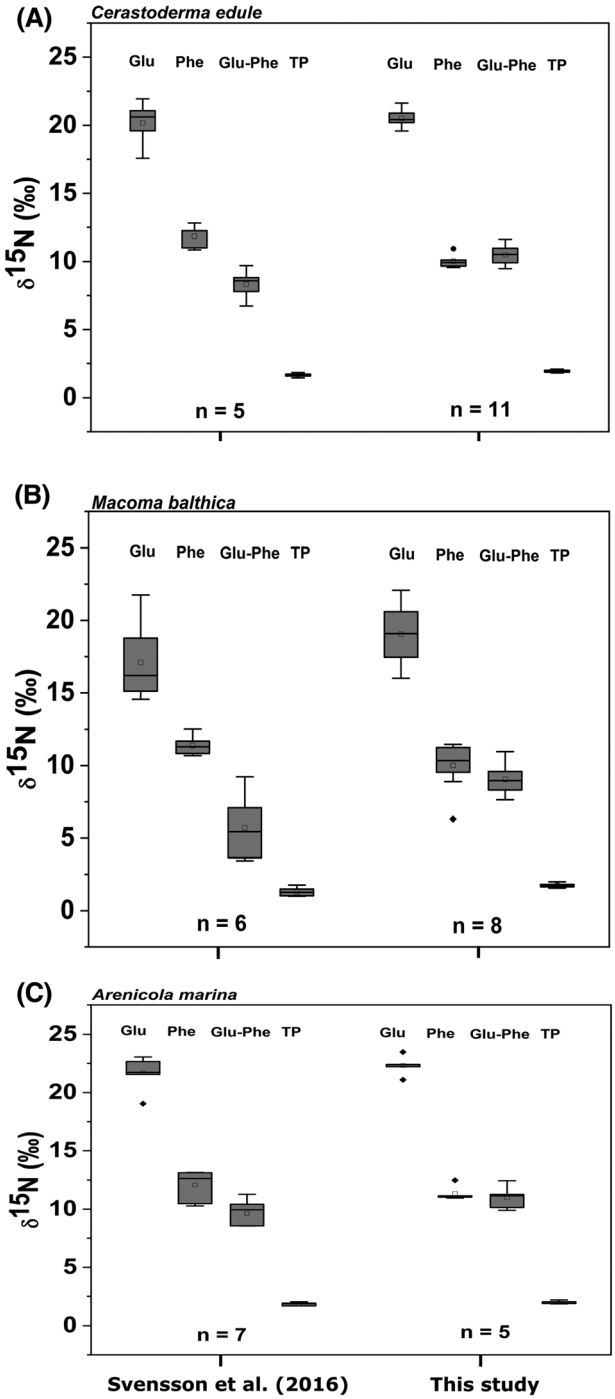

FIGURE 6 δ^{15}N values for glutamic acid (Glu), phenylalanine (Phe), Glu-Phe, and trophic position (TP) for A, *C. edule* (common cockle); B, *M. balthica* (Baltic clam); and C, *A. marina* (lugworm) analyzed using the method presented in this study and the previously used method (Svensson et al[24]). Note that TP is unitless and is shown between methods for a comparison of precision provided with the two measurement estimates disregarding the error associated with the trophic discrimination factor (7.6 ± 2.5‰) and β (3.4 ± 0.9) used to calculate TP. Within the boxplot, open squares represent the mean, lines represent the median, boxes represent the upper and lower quartiles, and whiskers represent the 1.5 quartile ranges. Any black squares outside of the whiskers are outliers and *n* refers to number of individuals analyzed

calibrated reference materials and will be comparable with similarly standardized measurements in other laboratories. Improvement in analytical precision and more widespread utilization of normalization to international standards will allow for better comparison between TPs of animals across ecosystems.

6 | OTHER APPLICATIONS

Improved precision allows for a finer resolution of δ^{15}N differences within source AAs that may result in a positive identification of smaller per mil shifts for basal resource utilization among populations.[29,35] Reduced analytical error will improve resolution of differences for source AAs in materials that are formed across an animal's lifetime such as baleen or otoliths, where resource shifts are likely to be incremental, resulting in small initial ‰ changes.[10] Improved resolution will benefit the construction of isoscapes, detailed mapping of isotope baselines for individual compounds across landscapes, allowing for a finer partitioning of regional differences in examined source AAs.[36,37] Decreased analytical error will improve resolution for equations utilizing multiple individual AA values (e.g., such as ΣV, an estimate of the amount of microbial resynthesis of AAs that potentially indicates reworking of detrital material within the ecosystem[1,18]). Finally, improved analytical precision and a wider use of compound-specific normalization to available international standards will decrease the variance associated with AA measurements and improve between-study comparisons and meta-analyses for studies using these techniques.

ACKNOWLEDGEMENTS

The authors thank students from the 2018 NIOZ Marine Master course for providing samples for analysis. They also thank Dieter Juchelka and Maria de Castro (Thermo Fisher Scientific, Bremen, Germany) for technical assistance following considerable downtime and Diane O'Brien (University of Alaska Fairbanks) and Christopher Yarnes (UC Davis) for encouraging output of a relatively user-specific method paper during discussion at ISOECOL 2018. In addition, this work benefited from participation in the ISOECOL 2018 workshop: Approaches to improve the reproducibility of amino acid stable isotope analyses.

ORCID

Philip M. Riekenberg https://orcid.org/0000-0002-6275-5762
Marcel van der Meer https://orcid.org/0000-0001-6454-1752
Stefan Schouten https://orcid.org/0000-0001-9200-8269

REFERENCES

1. Ohkouchi N, Chikaraishi Y, Close HG, et al. Advances in the application of amino acid nitrogen isotopic analysis in ecological and biogeochemical studies. *Org Geochem*. 2017;113:150-174.
2. Fuller BT, Petzke KJ. The dietary protein paradox and threonine 15 N-depletion: Pyridoxal-5′-phosphate enzyme activity as a mechanism for the δ^{15}N trophic level effect. *Rapid Commun Mass Spectrom*. 2017;31(8):705-718.

3. Li C, Jian Z, Jia G, Dang H, Wang J. Nitrogen fixation changes regulated by upper water structure in the South China Sea during the last two glacial cycles. *Global Biogeochem Cycles*. 2019;33(8):1010-1025.
4. Chikaraishi Y, Ogawa NO, Kashiyama Y, et al. Determination of aquatic food-web structure based on compound-specific nitrogen isotopic composition of amino acids. *Limnol Oceanogr Methods*. 2009; 7(11):740-750.
5. McClelland JW, Montoya JP. Trophic relationships and the nitrogen isotopic composition of amino acids in plankton. *Ecology*. 2002;83(8): 2173-2180.
6. Chikaraishi Y, Kashiyama Y, Ogawa NO, Kitazato H, Ohkouchi N. Metabolic control of nitrogen isotope composition of amino acids in macroalgae and gastropods implications for aquatic food web studies. *Mar Ecol Prog Ser*. 2007;342:85-90.
7. O'Connell TC. "Trophic" and "source" amino acids in trophic estimation: A likely metabolic explanation. *Oecologia*. 2017;184(2): 317-326.
8. Lorrain A, Graham BS, Popp BN, et al. Nitrogen isotopic baselines and implications for estimating foraging habitat and trophic position of yellowfin tuna in the Indian and Pacific oceans. *Deep-Sea Res II Top Stud Oceanogr*. 2015;113:188-198.
9. Vander Zanden HB, Arthur KE, Bolten AB, et al. Trophic ecology of a green turtle breeding population. *Mar Ecol Prog Ser*. 2013;476: 237-249.
10. Vane K, Wallsgrove NJ, Ekau W, Popp BN. Reconstructing lifetime nitrogen baselines and trophic position of *Cynoscion acoupa* from δ^{15}N values of amino acids in otoliths. *Mar Ecol Prog Ser*. 2018;597: 1-11.
11. Bradley Christina J, Wallsgrove Natalie J, Choy CA, et al. Trophic position estimates of marine teleosts using amino acid compound specific isotopic analysis. *Limnol Oceanogr Methods*. 2015;13(9): 476-493.
12. Nielsen JM, Popp BN, Winder M. Meta-analysis of amino acid stable nitrogen isotope ratios for estimating trophic position in marine organisms. *Oecologia*. 2015;178(3):631-642.
13. McMahon KW, McCarthy MD. Embracing variability in amino acid δ15N fractionation: Mechanisms, implications, and applications for trophic ecology. *Ecosphere*. 2016;7(12):1-26;e01511.
14. Yarnes CT, Herszage J. The relative influence of derivatization and normalization procedures on the compound-specific stable isotope analysis of nitrogen in amino acids. *Rapid Commun Mass Spectrom*. 2017;31(8):693-704.
15. Cowie GL, Hedges JI. Improved amino acid quantification in environmental samples: Charge-matched recovery standards and reduced analysis time. *Mar Chem*. 1992;37(3):223-238.
16. Metges CC, Petzke KJ. Measurement of15N/14 N isotopic composition in individual plasma free amino acids of human adults at natural abundance by gas chromatography–combustion isotope ratio mass spectrometry. *Anal Biochem*. 1997;247(1):158-164.
17. Takano Y, Kashiyama Y, Ogawa NO, Chikaraishi Y, Ohkouchi N. Isolation and desalting with cation-exchange chromatography for compound-specific nitrogen isotope analysis of amino acids: Application to biogeochemical samples. *Rapid Commun Mass Spectrom*. 2010;24(16):2317-2323.
18. McCarthy MD, Benner R, Lee C, Fogel ML. Amino acid nitrogen isotopic fractionation patterns as indicators of heterotrophy in plankton, particulate, and dissolved organic matter. *Geochim Cosmochim Acta*. 2007;71(19):4727-4744.
19. McCarthy MD, Lehman J, Kudela R. Compound-specific amino acid δ^{15}N patterns in marine algae: Tracer potential for cyanobacterial vs. eukaryotic organic nitrogen sources in the ocean. *Geochim Cosmochim Acta*. 2013;103:104-120.
20. McCarthy MD, Hedges JI, Bennar R. Major bacterial contribution to marine dissolved organic nitrogen. *Science*. 1998;281(5374):231-234.
21. Walsh RG, He S, Yarnes CT. Compound-specific δ^{13}C and δ^{15}N analysis of amino acids: A rapid, chloroformate-based method for ecological studies. *Rapid Commun Mass Spectrom*. 2014;28(1):96-108.
22. Christianen MJA, Middelburg JJ, Holthuijsen SJ, et al. Benthic primary producers are key to sustain the Wadden Sea food web: Stable carbon isotope analysis at landscape scale. *Ecology*. 2017;98(6):1498-1512.
23. Reinnicke S, Juchelka D, Steinbeiss S, Meyer A, Hilkert A, Elsner M. Gas chromatography/isotope ratio mass spectrometry of recalcitrant target compounds: Performance of different combustion reactors and strategies for standardization. *Rapid Commun Mass Spectrom*. 2012; 26(9):1053-1060.
24. Svensson E, Schouten S, Hopmans EC, Middelburg JJ, Sinninghe Damsté JS. Factors controlling the stable nitrogen isotopic composition (δ^{15}N) of lipids in marine animals. *PLoS ONE*. 2016;11(1): 1-12;e0146321.
25. Corr LT, Berstan R, Evershed RP. Optimisation of derivatisation procedures for the determination of δ13C values of amino acids by gas chromatography/combustion/isotope ratio mass spectrometry. *Rapid Commun Mass Spectrom*. 2007;21(23):3759-3771.
26. Schimmelmann A, Albertino A, Sauer PE, Qi H, Molinie R, Mesnard F. Nicotine, acetanilide and urea multi-level 2H-, 13C- and 15 N-abundance reference materials for continuous-flow isotope ratio mass spectrometry. *Rapid Commun Mass Spectrom*. 2009;23(22): 3513-3521.
27. Broek TAB, McCarthy MD. A new approach to δ^{15}N compound-specific amino acid trophic position measurements: Preparative high pressure liquid chromatography technique for purifying underivatized amino acids for stable isotope analysis. *Limnol Oceanogr Methods*. 2014;12(12):840-852.
28. Nielsen SL, Risgaard-Petersen N, Banta GT. Nitrogen retention in coastal marine sediments—A field study of the relative importance of biological and physical removal in a danish estuary. *Estuaries Coast*. 2017;40:1276-1287.
29. Vokhshoori NL, McCarthy MD, Collins PW, et al. Broader foraging range of ancient short-tailed albatross populations into California coastal waters based on bulk tissue and amino acid isotope analysis. *Mar Ecol Prog Ser*. 2019;610:1-13.
30. Brault EK, Koch PL, Costa DP, et al. Trophic position and foraging ecology of Ross, Weddell, and crabeater seals revealed by compound-specific isotope analysis. *Mar Ecol Prog Ser*. 2019;611: 1-18.
31. McMahon KW, Thorrold SR, Elsdon TS, McCarthy MD. Trophic discrimination of nitrogen stable isotopes in amino acids varies with diet quality in a marine fish. *Limnol Oceanogr*. 2015;60(3): 1076-1087.
32. Hare PE, Fogel ML, Stafford TW Jr, Mitchell AD, Hoering TC. The isotopic composition of carbon and nitrogen in individual amino acids isolated from modern and fossil proteins. *J Archaeol Sci*. 1991;18(3): 277-292.
33. Calleja ML, Batista F, Peacock M, Kudela R, McCarthy MD. Changes in compound specific δ^{15}N amino acid signatures and d/l ratios in marine dissolved organic matter induced by heterotrophic bacterial reworking. *Mar Chem*. 2013;149:32-44.
34. Webb EC, Lewis J, Shain A, et al. The influence of varying proportions of terrestrial and marine dietary protein on the stable carbon-isotope compositions of pig tissues from a controlled feeding experiment. *STAR: Sci Tech Archaeol Res*. 2017;3(1):28-44.
35. Madigan DJ, Chiang WC, Wallsgrove NJ, et al. Intrinsic tracers reveal recent foraging ecology of giant Pacific bluefin tuna at their primary spawning grounds. *Mar Ecol Prog Ser*. 2016;553:253-266.
36. Vokhshoori NL, McCarthy MD. Compound-specific δ^{15}N amino acid measurements in littoral mussels in the California upwelling ecosystem: A new approach to generating baseline δ^{15}N Isoscapes for coastal ecosystems. *PLoS ONE*. 2014;9(6):1-14;e98087.

37. McMahon KW, Newsome SD. Amino acid isotope analysis: A new frontier in studies of animal migration and foraging ecology. In: Hobson KA, Wassenaar LI, eds. *Tracking Animal Migration with Stable Isotopes*. 2nd ed. London: Academic Press; 2019:173-190.

SUPPORTING INFORMATION

Additional supporting information may be found online in the Supporting Information section at the end of this article.

How to cite this article: Riekenberg PM, van der Meer M, Schouten S. Practical considerations for improved reliability and precision during determination of $\delta^{15}N$ values in amino acids using a single combined oxidation–reduction reactor. *Rapid Commun Mass Spectrom*. 2020;34:e8797. https://doi.org/10.1002/rcm.8797